Available online at www.sciencedirect.com
ScienceDirect
Electric Power Systems Research 78 (2008) 97–105
ELECTRIC POWER SYSTEMS RESEARCH
www.elsevier.com/locate/epsr

Modeling and fault diagnosis of a photovoltaic system

Kuei-Hsiang Chao [a,*], Sheng-Han Ho [b], Meng-Hui Wang [a]

[a] *Department of Electrical Engineering, National Chin-Yi University of Technology, 35, Lane 215, Section 1, Chung-Shan Road, Taiping City 411, Taichung County, Taiwan, ROC*
[b] *Institute of Information and Electrical Energy, National Chin-Yi University of Technology, 35, Lane 215, Section 1, Chung-Shan Road, Taiping City 411, Taichung County, Taiwan, ROC*

Received 29 March 2006; received in revised form 6 December 2006; accepted 28 December 2006
Available online 20 February 2007

Abstract

In this paper, a circuit-based simulation model of a photovoltaic (PV) panel by PSIM software package is developed, firstly. Then, a 3 kW PV arrays established by using the proposed PSIM model with series and parallel connection is not only employed to carry out the fault analysis, but also to represent its *I–V* and *P–V* characteristics at variable surface temperatures and isolations under normal operation. Finally, a novel extension diagnosis method based on the extended correlation function and the matter-element model was proposed to identify the faulting types of a 3 kW PV system. The simulated results indicate that the proposed fault diagnosis method can detect the malfunction types correctly and promptly.

Keywords: Photovoltaic system; Fault diagnosis; Extension theory; PSIM software package

1. Introduction

Although the real-time simulation technique of the PV system has been developed in [1], it is still difficult to analyze the features of the PV system within the same atmosphere condition. Moreover, these techniques utilize an expensive solar simulator and their flexibilities are limited due to the construction of hardware. Numerous researchers have been trying to develop adequate simulation model by the simulation platforms for instance SPICE [2], SABER [3], and EMTP [4]. However, the combination of the PV system with varied series and parallel topology by using these simulation models cannot reveal the characteristics of the PV system. The simulated time is also an obstacle with these software platforms. Although the rate of calculation can be speeded up with the traditional mathematic model [5], the electrical behavior of the PV system still cannot be shown significantly. Furthermore, there are some simulation models being constructed with Neural Networks [6], Fuzzy [7] and Neural Fuzzy [8] algorithms for improving the simulated performance of the PV system, but an accurate model and expansibility of the PV system is still difficult to achieve.

With the related technology of photovoltaic (PV) systems rapidly growing, photovoltaic capability is increasing from an individual system (kW) to the power plant (MW). If the PV modules have a shading fault in one series of the connection branch, the shaded branch will actually be a burden that drains the generated power from the non-shaded solar modules. In addition, the shading situations may cause a so-called irreversible hot-spot damage to the cell, which causes focal-point heating with temperatures higher than 150 °C [9]. The PV system would be damaged under such shading effects over a long period of time [10]. Moreover, electrical accidents and module aging may also cause solar modules malfunction [11]. Meanwhile, PV modules are mismatched in terms of series connection with the transmission line resister which will lead to the output characteristics of PV modules greatly varying. Due to the continuous fault changes mentioned above, the output power and generation efficiency will fall.

Nowadays, since there is no supervisory mechanism for PV systems in a power level from 1 to 10 KW, thus, the exact faulting type identification is difficult for system operators. Therefore, traditional false diagnosis process causes a lot of time and manpower to be wasted in this search. What is more, the individual power plant (MW) runs at hundreds of volts, the maintenance could involve potential peril to employees. Hence, there is a need for diagnosing the PV system failure quickly and efficiently.

* Corresponding author. Tel.: +886 4 23924505x7272; fax: +886 4 23922156.
E-mail address: chaokh@ncut.edu.tw (K.-H. Chao).

0378-7796/$ – see front matter © 2007 Elsevier B.V. All rights reserved.
doi:10.1016/j.epsr.2006.12.012

A PSIM circuit-based model of the PV panel is presented in this paper for enhancing not only the less simulation time with large-scale PV arrays, but also showing the electrical behaviors of PV arrays for various topologies of series and parallel combination. In addition, a 3 kW photovoltaic arrays model was established to investigate the *I–V* and *P–V* characteristics and impacts of insolation, temperature and load varying. The PSIM model can be also used for further investigations, such as features of partial shadowing fault, module performance decayed analysis of PV panel, islanding analysis, etc. Furthermore, an extension diagnosis method based on the extended correlation function and the matter-element model was also proposed to identify the faulting types of the 3 kW PV system. The extension theory was proposed by Cai in 1983 for the purpose of solving inconsistent problems [12]. It has been adopted widely in many applications [13]. Nevertheless, the extension theory has seldom been employed in PV modules malfunction investigation. Since this theory allows classification problems with range features, analog input, discrete output, and without learning process, it is very suitable for PV fault diagnosis application. The matter-element model and extended mathematics are the main principles of extension theory. It can indicate the alterable relations between quality and quantity by matter-element transformation. The proposed fault diagnosis method will firstly create a set of fault matter-element of PV modules, and then a regular extended correction function will identify the fault type of PV arrays by calculating the degrees of extended correction. According to these results, the proposed fault diagnosis method detects the malfunction correctly and promptly with less memory consumption and the maintenance staffs can confirm the fault types of PV system without system interruption.

2. PSIM based solar module modeling

The solar cell is basically a p–n junction diode, and its traditional equivalent circuit may express itself similar to what is shown in Fig. 1 [6]. Where R_s is the very small series resistance and R_{sh} is the quite large shunt resistance. D_j is the ideal P–N diode, I_{ph} expressed as the photocurrent source generated proportionally by the surface temperature and insolation. V and I represent the output voltage and output current of the solar cell, respectively. According to the physical property of p–n semiconductor, the *I–V* characteristics of PV module could be expressed as follows [3]:

$$I\left(1+\frac{R_s}{R_{sh}}\right)=n_p I_{ph}-n_p I_{sat}\left[\exp\left\{\frac{q}{AkT}\left(\frac{V}{n_s}+IR_s\right)\right\}-1\right]-\frac{V-n_s}{R_{sh}} \quad (1)$$

In Eq. (1), q is the electron charge (1.602×10^{-19}, C); k represents the Boltzman constant (1.38×10^{-23} J/°K), T is the surface temperature of PV module and A shows the ideality factor ($A=1$–5). Where n_s is the number of cells connected in series and n_p is the number of cells parallelly connected. In addition, the module reverse saturation current I_{sat} shown in Eq. (2) varies with temperature T:

$$I_{sat}=I_{rr}\left(\frac{T}{T_r}\right)^3\exp\left\{\frac{qE_{gap}}{kA}\left(\frac{1}{T_r}-\frac{1}{T}\right)\right\} \quad (2)$$

E_{gap} is the energy of the band gap for silicon ($E_{gap}\cong1.1$ eV), and T_r is the reference temperature of solar cell. The I_{ph} expressed in Eq. (3) represents the photocurrent proportionally produced to the level of cell surface temperature and radiation. Where I_{sso} is the short-circuit current, k_i the short-circuit current temperature coefficient, and S_i is the solar radiation inW/m^2:

$$I_{ph}=\{I_{sso}+k_i(T-T_r)\}\frac{S_i}{1000} \quad (3)$$

A circuit-based SIEMENS SP75 solar module model will be formed from the PSIM software package. PSIM is a simulation software package especially designed for power electronics and motor control. It possesses the characteristics of fast speed and provides a powerful simulation environment for power electronics, analog and digital control, and motor drive systems [14]. The related specifications of SIEMENS SP75 can be found from the manufacturer datasheet [15]. In order to exhibit the influence of insolation and temperature, the tested scheme of PV module based on the PSIM software package is constructed as shown in Fig. 2. Eq. (1) is reproduced as the PSIM module and Eq. (3) is represented as 'Iph.dll block' in C-code to produce photocurrent I_{ph}. The variable parameters such as solar insolation and module surface temperature are included in the external DLL (dynamic link library) block, which allows users to write code in C/C++, and link it with PSIM. In addition, the "fault switch"

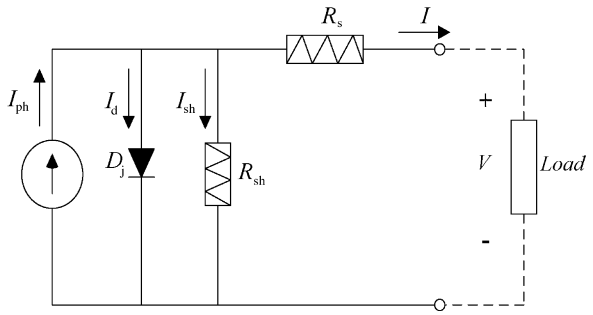

Fig. 1. The equivalent circuit of a solar cell.

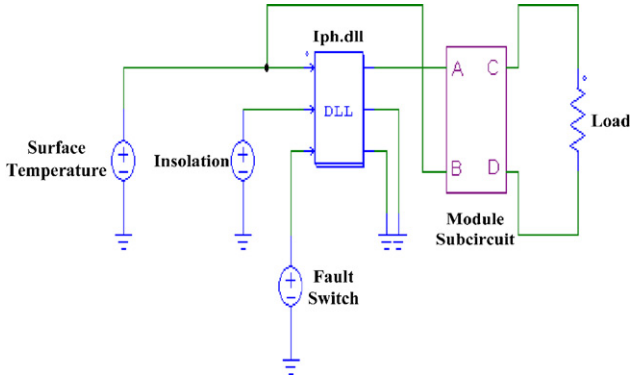

Fig. 2. The scheme diagram of PSIM based PV module.

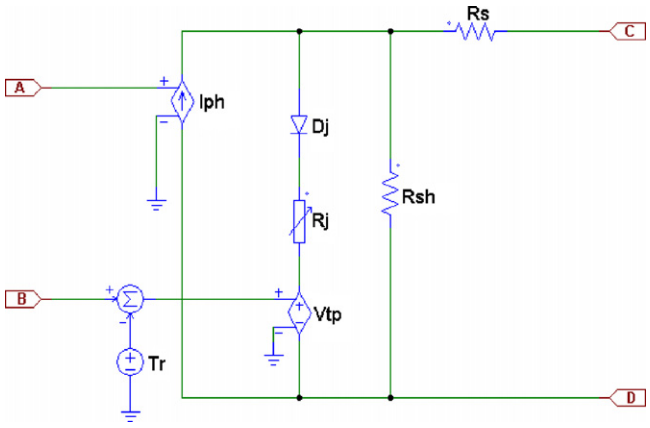

Fig. 3. The inner subcircuit of the proposed PV module.

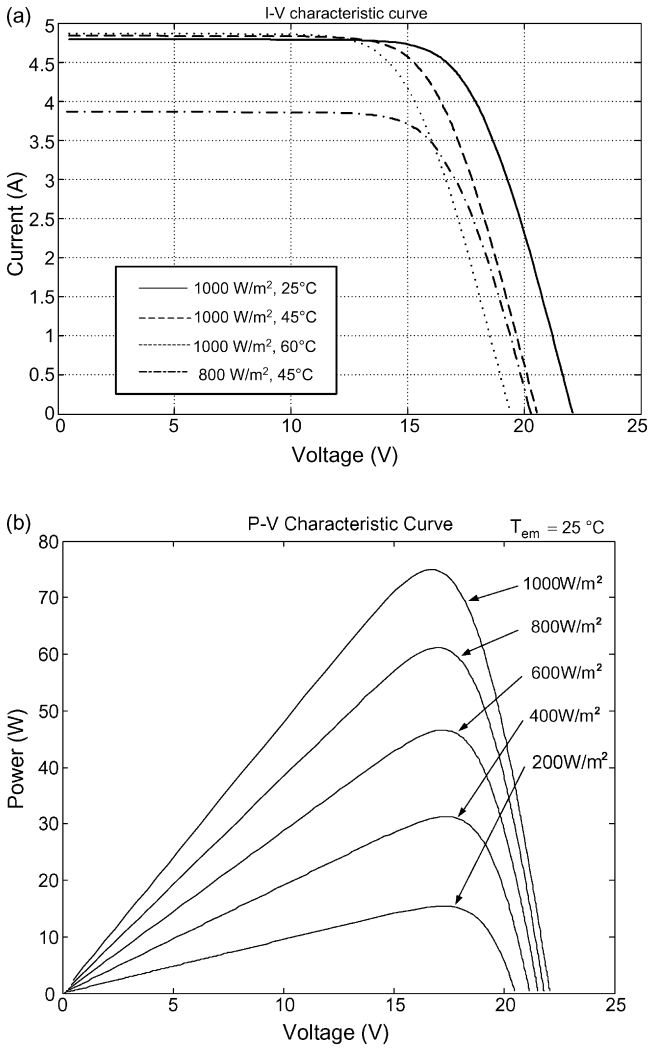

Fig. 4. The simulated characteristic curves of the proposed PSIM based PV model at variable irradiance and temperature: (a) *I–V* curve and (b) *P–V* curve.

could switch the proposed PSIM module to engage in faulting simulation or normal operation.

Fig. 3 shows the inner subcircuit of proposed PV module, where V_{tp} is the modified diode shield voltage as the temperature is changing, which can be expressed as Eq. (4), where k_v is the open-circuit voltage temperature coefficient:

$$V_{tp} = k_v(T - T_r) \tag{4}$$

Fig. 4(a) and (b) shows the simulated *I–V* and *P–V* characteristic curves of SIEMENS SP75 at variable irradiance and temperature by using the proposed PSIM model. It is clear that the simulated *I–V* and *P–V* characteristic curves are all close to those found from the manufacture datasheet of SIEMENS SP75 [15]. As we can see from Eq. (1), the photovoltaic current is a function of itself, causing an algebraic loop problem. For solving this problem, the series resistance is always neglected in conventional mathematical model to form a simple equation. Its results show that the proposed PSIM model can be significantly more accurate than the conventional model in simulating the PV module characteristics.

3. The summary of extension theory

In the Cantor set, an element either belongs to or does not belong to a set, so the range of the Cantor set is $\{0,1\}$, which can be used to solve a two-valued problem. In contrast to the standard set, the fuzzy set allows for the description of concepts in which the boundary is not explicit. It concerns not only whether an element belongs to the set but also to what degree it belongs to. The range of a fuzzy set is [0,1]. The extension set extends the fuzzy set from [0,1] to $(-\infty,\infty)$. As a result, it allows us to define a set that includes any data in the domain [12]. Extension theory tries to solve the incompatibility or contradiction problems by the transformation of the matter-element. The comparisons of the standard sets, fuzzy sets and extension sets are shown in Table 1. Some definitions of extension theory are introduced in the next section.

3.1. Matter-element model

The matter-element is one of the main theories in extension theory. A matter-element contains three essential factors. We can

Table 1
Three different sorts of mathematical sets

Compared item	Cantor set	Fuzzy set	Extension set
Research objects	Data variables	Linguistic variables	Contradictory problems
Model	Mathematics model	Fuzzy mathematics model	Matter-element model
Descriptive function	Transfer function	Membership function	Correlation function
Descriptive property	Precision	Ambiguity	Extension
Range of set	$C_A(x) \in (0,1)$	$\mu_A(x) \in [0,1]$	$K_A(x) \in (-\infty,\infty)$

define the matter with name N, whose characteristic is c, and v is the value related to c. The matter-element can be expressed as follows [12]:

$$R = (N \quad c \quad v) \tag{5}$$

where N, c, and v are called the three fundamental elements of the matter-element. For example, R = (John, weight, 90 kg) can be used to state that John's weight is 90 kg. In addition, we can assign the $R = (N \quad C \quad V)$ as a multi-dimensional matter-element with a characteristic vector $C = [c_1 \quad c_2 \quad \ldots \quad c_n]$ and the value vector $V = [v_1 \quad v_2 \quad \ldots \quad v_n]$ with respect to C. The multi-dimensional matter-element is described as

$$R = (N \quad C \quad V) = \begin{bmatrix} R_1 \\ R_2 \\ \vdots \\ R_n \end{bmatrix} = \begin{bmatrix} N & c_1 & v_1 \\ & c_2 & v_2 \\ & \vdots & \vdots \\ & c_n & v_n \end{bmatrix} \tag{6}$$

In Eq. (6), $R_j = (N \quad c_j \quad v_j)$ ($j = 1, 2, \ldots, n$) is the sub-matter-element of R. Based on the matter-element model, a new mathematical concept can be established to characterize the relationship between the quality and quantity of a matter by matter-element model.

3.2. Conception of extension set

Set theory is a kind of mathematical scheme that describes the classification and pattern recognition about an objective. A Cantor set describes the definiteness of matters; a fuzzy set describes the fuzziness of matters. The extension set extends the fuzzy set from [0,1] to $(-\infty,\infty)$ [12]. An extension set is composed of two definitions.

Definition 1. Let U be a space of objects and x a generic element of U, then an extension set $\tilde{E}$ in U is defined as a set of ordered pairs as follows:

$$\tilde{E} = \{(x, y) | x \in U, y = K(x) \in (-\infty, \infty)\} \tag{7}$$

where $y = K(x)$ is called the correlation function for extension set $\tilde{E}$. The $K(x)$ maps each element of U to a membership grade between $-\infty$ and ∞. An extension set $\tilde{E}$ in U can be denoted by

$$\tilde{E} = E^+ \cup Z_0 \cup E^- \tag{8}$$

where

$$E^+ = \{(x, y) | x \in U, y = K(x) > 0\} \tag{9}$$

$$Z_0 = \{(x, y) | x \in U, y = K(x) = 0\} \tag{10}$$

$$E^- = \{(x, y) | x \in U, y = K(x) < 0\} \tag{11}$$

In Eqs. (9)–(11), E^+, E^- and Z_0 are called, respectively, the positive field, negative field and zero boundary in $\tilde{E}$.

Definition 2. If $X_0 = \langle a,b \rangle$, and $X = \langle f,g \rangle$, are two intervals in the real number field, and $X_0 \subset X$, where X_0 and X are the classical (concerned) and neighborhood domains, respectively. The correlation function in the extension theory can be defined as follows:

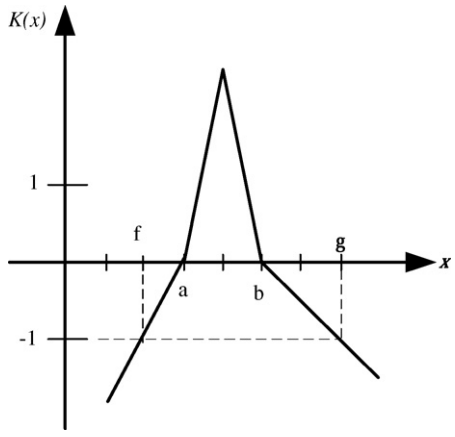

Fig. 5. The correlation functions of the proposed diagnosis method.

$$K(x) = \begin{cases} -\rho(x, X_0) & x \in X_0 \\ \dfrac{\rho(x, X_0)}{\rho(x, X) - \rho(x, X_0)} & x \notin X_0 \end{cases} \tag{12}$$

where

$$\rho(x, X_0) = \left| x - \frac{a+b}{2} \right| - \frac{b-a}{2} \tag{13}$$

$$\rho(x, X) = \left| x - \frac{f+g}{2} \right| - \frac{g-f}{2} \tag{14}$$

The correlation function can be used to calculate the membership grade between x and X_0. The extended membership function is shown in Fig. 5. When $K(x) \geq 0$, it indicates the degrees to which x belongs to X_0. When $K(x) < 0$ it describes the degree to which x does not belong to X_0. When $-1 < K(x) < 0$, it is called the extension domain, which means that the element x still has a chance to become part of the set if conditions change.

4. The proposed faulting diagnosis method

A 3 kW photovoltaic arrays model with 4 × 40 series–parallel connection can be constructed by the circuit-based PSIM model of single PV module. The PV system generates a maximum power of 2992 W at 68 V rated output voltage and 44 A rated output current. Fig. 6 shows the I–V and P–V characteristic curves of the established 3 kW PV arrays. To simulate the "Module Fault" in the PV system, the fault switch located at the PV system can be firstly selected, then setting the amount of faulting PV panels and assigning the insolation and temperature to simulate the module fault operation.

The output voltage, current, and power will differ at varied atmosphere in all fault categories when failure continuously changed. Consequently, the proposed fault diagnosis method divides atmosphere into seven sections according to the average temperature and relative irradiation in Taiwan [16]. The distinguishable specification of the atmosphere sections represents as Fig. 7. Sections C–G are the atmosphere conditions for the most PV system operation. A and B sections represent the

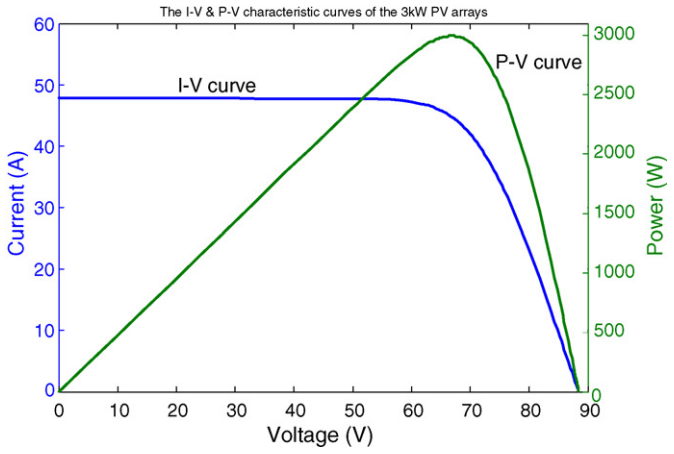

Fig. 6. The simulated *I–V* and *P–V* characteristic curves of the 3 kW PV arrays.

insufficient irradiation region. Moreover, the extension diagnosis method establishes the matter-element model for all faulting sorts in every atmosphere region. The output power, voltage, and current of PV system are regarded as the characteristics of the matter-element in the proposed method.

In the process of the proposed method, the atmosphere sections will discriminate firstly when malfunction takes place. Following this, the detector measures the three characteristic values and delivers it to the proposed malfunction investigation system. Finally, the fault category will be recognized by selecting the maximum value of all relation degree indices. According to the recognized result, the maintained staff can find up the amount of panels that broke down and proceed with troubleshooting.

4.1. Matter-element model of fault categories

Based on the proposed diagnosis method, the faulting categories can be divided into six kinds. The represented symbols of these fault categories are described below:

- PF_1. Normal operation.
- PF_2. Any 1 branch with 1 module fault in 10 series of connection branches.

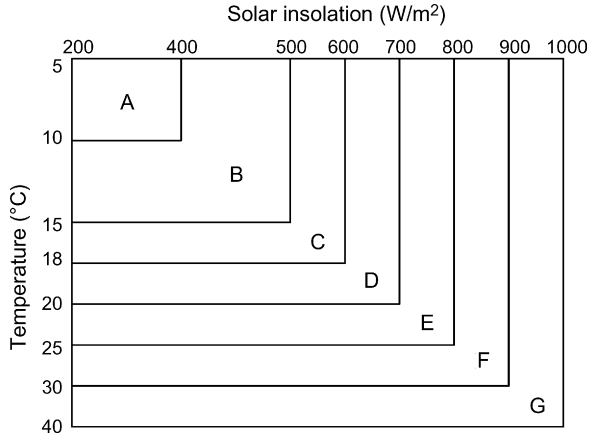

Fig. 7. The distinguishable specification of the atmosphere sections.

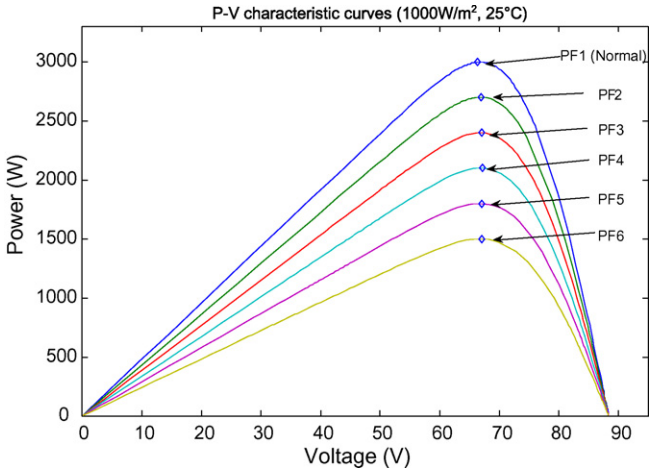

Fig. 8. The output power of PV array system when module failure happened at the standard test conditions (STC).

- PF_3. Any 2 branches with 1 module fault in 10 series of connection branches.
- PF_4. Any 3 branches with 1 module fault in 10 series of connection branches.
- PF_5. Any 4 branches with 1 module fault in 10 series of connection branches.
- PF_6. Any 5 branches with 1 module fault in 10 series of connection branches.

Fig. 8 indicates that the power output degrades rapidly when module failure happened at Standard Test Conditions (STC, irradiation is 1000 W/m^2, temperature is 25 °C). According to the simulated results, the faulting matter-element of atmosphere section G within insolation 901–1000 W/m^{2}and temperature 30–40 °C are shown in Table 2. PF = {PF_1, PF_2, PF_3, . . ., PF_6}

Table 2
The fault matter-element model of atmosphere section G within isolation 901–1000 W/m^2 and temperature 30–40 °C

Fault types	Matter-element model
PF_1	$R_{F1} = \begin{Bmatrix} P_{F1} & v_{out} & \langle 62.8, 67.0\rangle \\ & i_{out} & \langle 40.6, 43.4\rangle \\ & p_{out} & \langle 2558.0, 2904.9\rangle \end{Bmatrix}$
PF_2	$R_{F2} = \begin{Bmatrix} P_{F2} & v_{out} & \langle 58.8, 63.6\rangle \\ & i_{out} & \langle 38.1, 41.2\rangle \\ & p_{out} & \langle 2244.5, 2621.9\rangle \end{Bmatrix}$
PF_3	$R_{F3} = \begin{Bmatrix} P_{F3} & v_{out} & \langle 53.3, 58.5\rangle \\ & i_{out} & \langle 34.4, 37.8\rangle \\ & p_{out} & \langle 1838.7, 2218.2\rangle \end{Bmatrix}$
PF_4	$R_{F4} = \begin{Bmatrix} P_{F4} & v_{out} & \langle 46.8, 51.9\rangle \\ & i_{out} & \langle 30.3, 33.6\rangle \\ & p_{out} & \langle 1417.9, 1742.9\rangle \end{Bmatrix}$
PF_5	$R_{F5} = \begin{Bmatrix} P_{F5} & v_{out} & \langle 40.2, 44.7\rangle \\ & i_{out} & \langle 26.0, 28.9\rangle \\ & p_{out} & \langle 1047.5, 1295.5\rangle \end{Bmatrix}$
PF_6	$R_{F6} = \begin{Bmatrix} P_{F6} & v_{out} & \langle 33.6, 37.4\rangle \\ & i_{out} & \langle 21.7, 24.2\rangle \\ & p_{out} & \langle 732.9, 906.3\rangle \end{Bmatrix}$

is the fault set and PF_n denotes the nth faulting sort. The "Normal operation" is simulated for confirming that the proposed method can correctly identify the PV system is whether in normal operation or malfunctioning. The classical regions and value range of every characteristic are assigned by the lower and upper boundary of simulated records. In addition, one can set a matter-element model to express the neighborhood domain of every characteristic for describing the possible range of all fault set. The value range of neighborhood domain $V'_F = \langle f, g\rangle$ could be determined from the maximum and minimum values of every characteristic in simulated records. This can be represented as

$$R_F = (P_F \quad C \quad V'_F) = \begin{Bmatrix} P_F & V_{out} & \langle 21, 53\rangle \\ & i_{out} & \langle 13, 35\rangle \\ & p_{out} & \langle 326, 1722\rangle \end{Bmatrix} \tag{15}$$

4.2. The diagnostic procedure of the proposed method

The proposed diagnosis method can be dealt with by the computer program. The process of the proposed method is shown as below:

- *Step 1*. Establishing the matter-element model of every faulting category in every section, which is performed as follows:

$$R_{Fj} = \begin{bmatrix} R_{Fj} & V_{out} & V_{j1} \\ & I_{out} & V_{j2} \\ & p_{out} & V_{j3} \end{bmatrix}, \quad j = 1, 2, \ldots, 6 \tag{16}$$

  where $V_{jk} = \langle a_{jk}, b_{jk}\rangle$ is the classical region of every characteristic set. In this paper, the classical region of each fault matter-element is assigned by the maximum and minimum values of output voltage, current, and power.
- *Step 2*. Setting the matter-element of the tested PV modules as follows:

$$R_{Fx} = (P_{Fx} \quad C \quad V_F) = \begin{Bmatrix} P_{Fx} & v_{out} & v_{f1} \\ & i_{out} & v_{f2} \\ & p_{out} & v_{f3} \end{Bmatrix} \tag{17}$$

- *Step 3*. Calculating the correlation degrees of the tested PV modules with the characteristic of each fault matter-element by the proposed extended correlation function as follows:

$$K_{jk}(v_{fk}) = \begin{cases} \dfrac{-\rho(v_{fk}, V_{jk})}{|V_{jk}|} & \text{if } v_{fk} \in V_{jk} \\ \dfrac{\rho(v_{fk}, V_{jk})}{\rho(v_{fk}, V'_{jk}) - \rho(v_{fk}, V_{jk})} & \text{if } v_{fk} \notin V_{jk} \end{cases} \quad \text{for } f = 1, 2, 3, \ldots, 6; k = 1, 2, 3 \tag{18}$$

  where

$$|V_{jk}| = \left|\frac{b_{jk} - a_{jk}}{2}\right| \tag{19}$$

$$\rho(v_{fk}, V_{jk}) = \left|v_{fk} - \frac{a_{jk} + b_{jk}}{2}\right| - \frac{1}{2}(b_{jk} - a_{jk}) \tag{20}$$

$$\rho(v_{fk}, V'_{jk}) = \left|v_{fk} - \frac{f_{jk} + g_{jk}}{2}\right| - \frac{1}{2}(g_{jk} - f_{jk}) \tag{21}$$

- *Step 4*. Assigning weights to the faulting characteristic such as W_{j1}, W_{j2}, W_{j3}, denoting the significance of every faulting characteristic. In this paper, W_{j1}, W_{j2}, W_{j3} are set as 1/3 because the significance of these three characteristics are equal.
- *Step 5*. Calculating the relation degrees of every faulting category:

$$\lambda_j = \sum_{k=1}^{3} W_{jk} K_{jk} \quad (j = 1, 2, 3, \ldots, 6) \tag{22}$$

- *Step 6*. Normalizing the relation degrees for every fault category to be between 1 and −1. This procedure will conveniently diagnose the faulting category:

$$\lambda'_j = \begin{cases} \dfrac{\lambda_j}{|\lambda_{max}|} & \text{if } \lambda_j > 0 \\ \dfrac{\lambda_j}{|-\lambda_{max}|} & \text{if } \lambda_j < 0 \end{cases} \tag{23}$$

- *Step 7*. Selecting the maximum value from the normal relation degrees (or 1) to recognize the faulting category of the tested PV module. The judgmatical equation is shown as follows:

$$\text{if } (\lambda'_j = 1), \text{ then } (PF_x = PF_j) \tag{24}$$

  The fault indices obtained from the proposed diagnosis method not only point out the accuracy of the main fault type compared to the other, but also indicate the fault probability of other categories. In general, the more relation index values that are owned, the greater possibility of a fault to occur.
- *Step 8*. If a new tested PV module exists, then go back to Step 2, or else end the process.

5. Simulated results

Firstly, the fault records in atmosphere section G are selected to test the effectiveness of the proposed extension fault diagnosis method. Table 3 lists eight tested data selected arbitrarily from the fault records in atmosphere section G. The input parameters of PV arrays system in every atmosphere section include insolation, temperature and the numbers of fault switch. Whereas, their output signals are voltage, current and power, which are also considered as the tested parameters in the diagnosis process. Table 4 shows the identified results of the proposed method with the fault relation indices λ'_j for each fault type. Compared to the tested data listed in Table 3, it demonstrates that the proposed diagnosis method can correctly recognize the fault category. For instance, in tested number 2, the relation index is 1 (or maximum value) for the fault category PF_1. It indicates that the PV arrays system is now working properly in atmosphere section G. Moreover, the relation indexes of other fault category are all

Table 3
The tested data obtained in atmosphere section G

Tested no.	Insolation (W/m^2)	Temperature (°C)	The number of fault switch	Voltage (V)	Current (A)	Power (W)	Faulting types
1	917	37	4	41.0	26.5	1086.5	PF_5
2	983	31	0	66.6	43.1	2878.4	PF_1
3	950	33	4	49.3	31.9	1572.6	PF_5
4	928	38	5	34.7	22.4	777.3	PF_6
5	931	32	2	54.9	35.5	1948.9	PF_3
6	998	36	3	51.7	33.5	1731.9	PF_4
7	946	34	1	61.3	39.7	2433.6	PF_2
8	905	35	3	47.1	30.4	1431.8	PF_4

Table 4
The identified results of the proposed method in atmosphere section G

Tested no.	Relation indexes λ'_j of fault types						Section	Result
	PF_1	PF_2	PF_3	PF_4	PF_5	PF_6		
1	−1	−0.935	−0.191	−0.537	1	−0.381	G	PF_5
2	1	−0.629	−0.834	−0.927	−0.973	−1	G	PF_1
3	−1	−0.809	−0.421	−0.278	1	−0.803	G	PF_5
4	−1	−0.98	−0.942	−0.863	−0.690	1	G	PF_6
5	−0.669	−0.40	1	−0.324	−0.759	−1	G	PF_3
6	−0.904	−0.671	−0.184	1	−0.644	−1	G	PF_4
7	−0.226	1	−0.35	−0.726	−0.902	−1	G	PF_2
8	−1	−0.856	−0.566	1	−0.254	−0.726	G	PF_4

Table 5
The tested instances of PV system selected from A to G atmosphere sections

Tested no.	Insolation (W/m^2)	Temperature (°C)	The number of fault switch	Voltage (V)	Current (A)	Power (W)	Atmosphere section	Faulting types
1	1000	37	3	51.9	33.6	1742.3	G	PF_4
2	850	26	0	61.8	40.0	2476.7	F	PF_1
3	680	19	4	30.3	19.6	594.9	D	PF_5
4	510	17	2	30.1	19.5	588.6	C	PF_3
5	770	23	1	51.1	33.1	1692.8	E	PF_2
6	570	16	5	21.3	13.8	295.0	C	PF_6
7	430	12	2	25.4	16.4	417.8	B	PF_3
8	310	8	1	20.5	13.3	272.8	A	PF_2

negative values, which mean that the possibility on other fault category is much lower than the fault category PF_1.

In addition, the field tested instances of PV system between A and G atmosphere sections shown in Table 5 are also selected to reveal the flexibility of the proposed fault diagnosis method. Table 6 represents the simulated results of six fault types can be identified exactly in large field sections. Furthermore, the proposed method can indicate the atmospheric section which the tested instance belongs to as well. The proposed extension fault diagnosis method does not only diagnose the main fault category of the PV system, but can also diagnose that the possibilities of other fault categories have been revealed by the relation indices.

Table 6
The identified results of PV system obtained from A to G atmosphere sections

Tested no.	Relation indexes of each fault type						Section	Diagnostic result
	PF_1	PF_2	PF_3	PF_4	PF_5	PF_6		
1	−1	−0.737	−0.191	1	−0.354	−0.968	G	PF_4
2	1	−0.435	−0.778	−0.901	−0.963	−1	F	PF_1
3	−1	−0.134	0.146	0.399	1	0.325	D	PF_5
4	0.006	0.351	1	0.175	−0.504	−1	C	PF_3
5	−0.084	1	0.025	−0.580	−0.861	−1	E	PF_2
6	−1	−0.985	−0.962	−0.919	−0.814	1	C	PF_6
7	−0.053	0.275	1	0.089	−0.761	−0.962	B	PF_3
8	0.401	1	0.369	0.005	−0.601	−0.872	A	PF_2

Table 7
The comparison of the classification accuracy rate for different methods

Method	The number of iteration	The amount of constructed (or learning) data	The amount of tested data	Identification accuracy rate (%)
The proposed extension method	0	12	6000	99.11
MLP-BP (3-6-6-6)	1500 (epochs)	6000	6000	97.01
K-Means	500	6000	6000	75.183

Table 8
The identification accuracy rate in every atmosphere section

Atmosphere section	Accuracy rate (%)
A	95.879
B	96.011
C	96.350
D	97.946
E	98.838
F	99.792
G	99.117

For example, the relation index of PF_4 is 0.399 in tested number 3, which means that the PV system has a 39.9% possibility on fault category PF_4. In addition, the tested number 4 has the lowest possibility for PF_1, because its relation index is -1 (or minimum). This information will be useful to find the hidden fault of the tested object for a maintenance engineer.

To prove the efficiency of the proposed method, the comparison of the classification accuracy rate with MLP-BP (Multilayer Perceptron-Back Propagation) [17] and K-Means clustering [18] are also shown in Table 7. It shows that the atmosphere section G includes a total of 6000 instances, which were used to train the MLP-BP network with 2 hidden layers and 90 connections. In addition, the K-Means clustering classifies these 6000 sets with 500 iterations, too. Table 7 indicates that the proposed method has a higher accuracy rate than others, where the proposed method has accuracy of 99% in 6000 tested instances. Contrarily, the accuracy of a MLP-BP method and K-Means clustering are, respectively, only 97% and 75% in the same conditions. Moreover, the proposed method does not need learning procedure, but only using 12 instances to find the low bound and upper bound of the input features. It is rather beneficial when implementing the proposed fault diagnosis method in a microcomputer for a real-time fault detecting device or a portable instrument. The identification accuracy rate of every atmosphere section by the proposed fault diagnosis method is also listed in Table 8. The results verify that the proposed method has high accuracy rate about 95–99% under different testing conditions.

6. Conclusion

In this paper, an accurate circuit-based PV module was established by the PSIM software package, which combined a 3 kW PV arrays system as well as gathered the tested data for fault diagnosis. According to the compared results, the proposed PSIM based PV module possesses a higher accuracy in electrical parameters than the conventional mathematic model. Furthermore, the simulated results also show that the proposed fault diagnosis method can easily recognize the main fault category and indicate the possibilities of others. The less constructed data utilized, no learning procedures needed and high identification rate; these are the good features of the proposed fault diagnosis method. When the capacity of the PV system increases, only a fractional amount of the data should be modified, thus the update interval may be much reduced. Therefore, the proposed method will be easy to implement in a real-time fault detecting device or a portable instrument. The proposed method also has good economic benefits for the maintenance of large-scale PV arrays system with MW power plant capacity in the future.

Appendix A

List of symbols

A	ideality factor ($A = 1$–5) of solar cell
C	characteristic vector of multi-dimensional matter-element
$\tilde{E}$	a set of systematic pairs in U
E_{gap}	band gap energy for silicon $\cong 1.1$ eV
I	output current of PV module
I_{ph}	photocurrent of PV module
I_{rr}	reverse saturation current at temperature 25 °C, irradiation 1000 W/m^2
I_{sat}	diode reverse saturation current of solar cell model
I_{sso}	short-circuit current at temperature 25 °C, irradiation 1000 W/m^2
k	Boltzman's constant $\cong 1.38 \times 10^{-23}$ J/°K
K_i	short-circuit current temperature coefficient
K_v	open-circuit voltage temperature coefficient
n_p	number of cells connected in parallel
n_s	number of cells connected in series
N	name for matter-element
q	electron charge $\cong 1.602 \times 10^{-19}$ C
R_j	sub-matter-element of multi-dimensional matter-element
R_s	series resistance of solar cell model
R_{sh}	shunt resistance of solar cell model
S_i	solar radiation
T	surface temperature of PV module
T_r	reference temperature of solar cell
U	an universe set of the extension set
V	output voltage of PV module
$\boldsymbol{V}$	value vector of multi-dimensional matter-element
V_{jk}	the classical domain of every characteristic set
V_{tp}	modified diode shield voltage
V'_{jk}	the neighborhood domain of every characteristic set

W_{jk} the weighting factor of the faulting category
X neighborhood domain of primitively extended correlation
X_0 classical domain of primitively extended correlation

References

[1] M. Park, Y. In-Keun, A novel real-time simulation technique of photovoltaic generation system using RTDS, IEEE Trans. Energy Convers. 19 (1) (2004) 164–169.

[2] F.D. No, T.D. Morgan, SPICE-modeling of cascade solar cells, in: Proceedings of the IEEE Southeast Conference, 1991, pp. 776–780.

[3] J.A. Gow, C.D. Manning, Development of photovoltaic array model for use in power-electronics simulation studies, IEE Proc. Electric Power Appl. 146 (2) (1999) 193–200.

[4] K.W. Horng, Measurement and EMTP modeling of photovoltaic cells applied to the analysis of partial shading faults, Master Thesis, National Yunlin University of Science & Technology, Taiwan, 2003.

[5] J.H.R. Enslin, D.B. Snyman, Combined low-cost, high-3 efficient inverter, peak power tracker and regulator for PV applications, IEEE Trans. Power Electron. 6 (1) (1991) 73–82.

[6] A. AI-Amoudi, L. Zhang, Application of radial basis function networks for solar-array modeling and maximum power-point prediction, IEE Proc. Gener. Transm. Distrib. 147 (5) (2000).

[7] Th.F. Elshatter, M.T. Elhagry, E.M. Abou-Elzahab, A.A.T. Elkousy, Fuzzy modeling of photovoltaic panel equivalent circuit, in: Proceedings of the Photovoltaic Specialists Conference, vol. 15, no. 22, 2000, pp. 1656–1659.

[8] M. AbdulHadi, A.M. Al-Ibrahim, G.S. Virk, Neuro-fuzzy-based solar cell model, IEEE Trans. Energy Convers. 19 (3) (2004) 619–624.

[9] W. Herrmann, W. Wiesner, W. VaaBen, Hot spot investigations on PV modules-new concepts for a test standard and consequences for modules design with respect to bypass diode, in: Proceedings of the IEEE Photovoltaic Specialists Conference, 1997, pp. 1129–1132.

[10] V. Quaschning, R. Hanitsch, Influence of shading on electrical parameters of solar cells, in: Proceedings of the 25th Photovoltaic Specialists Conference, 1996, pp. 1287–1290.

[11] V. Saly, M. Ruzinsky, P. Redi, Indoor study and ageing tests of solar cells and encapsulations of experimental modules, in: Proceedings of the 24th International Spring Seminar on Electronics Technology, 2001, pp. 59–62.

[12] W. Cai, The extension set and incompatibility problem, J. Sci. Explor. 1 (1983) 81–93.

[13] Y.P. Huang, H.J. Chen, The extension-based fuzzy modeling method and its applications, in: Proceedings of the IEEE Canadian Conference on Electrical and Computer Engineering, 1999, pp. 977–982.

[14] PSIM User's Guide, Powersim Inc., 2001–2003.

[15] SIEMENS Solar Module SP75 Specifications, Siemens Solar Industries, 2002.

[16] T.H. Hsu, Research in the solar radiation of Taiwan and the potential of solar powered energy generator, Master Thesis, National Taiwan Normal University, Taiwan, 2002.

[17] M.T. Hagen, H.B. Demuth, M.H. Beale, Neural Network Design, Thomson Learning, Boston, 1996.

[18] R.O. Dude, P.E. Hart, Pattern Classification and Scene Analysis, Wiley, New York, 1973.